Bed Nonhomogeneity in Turbulent Gas-Solid Fluidization

Bing Du, W. Warsito, and Liang-Shih Fan
Dept. of Chemical Engineering, The Ohio State University, Columbus, OH 43210

Bed dynamic behavior in a gas-solid fluidization system is measured in real time using ECT based on the NNMOIRT recently developed. The ECT results reveal the time-averaged and transient characteristics of the bubble/void phase and the emulsion phase, which is of value to the verification of the 3-D computation codes with real physical systems. In the turbulent regime, the time-averaged solids holdup distribution exhibits radial symmetry, which is not the case for the bubbling regime. The standard deviations of the fluctuations of the cross-sectional, averaged bubble/void phase fraction, and the cross-sectional, averaged solids holdups in the bubble/void phase and in the emulsion phase, all peak at the transition velocity from the bubbling to the turbulent regimes U_c. The addition of 10% fine particles decreases the solids holdup in the emulsion phase due to the breakup of large bubbles. The ECT study indicates that optical fiber probe measurement of the bubble/void phase fraction may yield significantly different results depending on the threshold level selected for the measured solids holdup distribution. The bubble/void phase fraction measured by the optical fiber probe does not vary with bed temperature up to 400°C; the emulsion phase voidage is observed to increase as the bed temperature increases.

Introduction

The turbulent fluidization regime, bound between the bubbling and the fast fluidization regimes, is characterized by vigorous movements of both the particles/clusters and bubbles/voids of irregular shapes. The resulting extensive mixing behavior and high solids holdups are appealing for fluidized beds to be operated under this regime for chemical reactor applications. The hydrodynamics of turbulent fluidization have been investigated to some extent (Bi et al., 2000). However, much remains to be known about this regime. This study is intended to probe the fundamental understanding of the nonhomogeneity of the flow structure in turbulent fluidization. Experiments are performed to shed light on this aspect.

Numerous intrusive, as well as nonintrusive, techniques have been used for measuring the hydrodynamic behavior of a gas-solids fluidized bed. The intrusive techniques are widely used for local property measurement in the fluidized beds. These techniques include the momentum probe, the capacitance probe, and the optical fiber probe.

The momentum probe is applied by measuring the pressure drop between the apertures of two tubes, facing the upstream and downstream flow in the bed (Azzi et al., 1991; Zhang et al., 1994; Bai et al., 1996). To prevent particle blockage in the tube, which often occurs in fluidization with high solids holdups, purging gas is usually introduced to clear the blockage. To obtain quantitative information of the flow structure in a fluidized bed, other measurements such as solids flux or solids concentration should be conducted.

Capacitance probes are utilized to measure the local solids holdup based on the local dielectricity of the gas-solids suspension (Yates and Simons, 1994; Werther, 1999). The technique has been applied to measure the local solids holdup and velocity in circulating fluidized-bed (CFB) systems (Brereton and Grace, 1993; Hage et al., 1996; Wiesendorf and Werther, 2000). Abed (1984) investigated the hydrodynamics in the turbulent fluidized bed using a capacitance probe. Werther and Wein (1994) measured the local solids holdup in two pilot-scale fluidized beds using the needle-type capacitance probes. They reported no significant change in the fluidization characteristics as the gas velocity increased from the bubbling to the turbulent regimes. However, there

Correspondence concerning this article should be addressed to L.-S. Fan.

are problems with the capacitance probe technique. The capacitance probe is sensitive to electrostatic effects and influenced by the changes in temperature and relative humidity. Furthermore, the measuring volume is relatively difficult to define.

The optical fiber probe technique measures the reflective light intensity by the solids in the bed. With this technique, the measuring volume of the optical fiber probe is often not well defined. Further, the measuring volume varies with the solids holdup in the bed, introducing error into the measurement by this technique. A reliable and precise calibration is essential for this technique. Nakajima et al. (1991) measured the bubble phase fraction and the voidage in the emulsion phase in the transition to the turbulent fluidization regime. They found that in the turbulent regime, the bubble fraction increased slightly with increasing gas velocity and also that the emulsion phase expanded more in the turbulent regime than in the bubbling regime. Lin et al. (2001) analyzed the transient density signal measured by the optical fiber probe and reported the two-phase microstructure flow in all gas-solid fluidization regimes. Zhang et al. (1997) and Bayle et al. (2001) studied the bubble characteristics in a turbulent fluidized bed using an optical fiber probe. Cui et al. (2001) studied the dynamic two-phase flow structure in fluidized beds based on a statistical analysis of optical fiber probe data. All these probes can only measure the flow behavior locally. Few measurements have been made on the global bed dynamic behavior; this is hindering a better understanding of the macroscopic interactive characteristics between the bubble/void phase and the emulsion phase and flow structure. Nonintrusive techniques can be utilized to perform such measurements.

The pressure transducer is the simplest nonintrusive technique used to study the global dynamic behavior of gas and solids in the bed. Pressure fluctuations have been successfully used to determine the transition velocity, U_c (Yerushalmi and Cankurt, 1979). The process tomography is an important nonintrusive technique that utilizes remote sensors to obtain time-averaged or real-time field images. A number of tomography techniques, such as X-ray, γ-ray, optical, ultrasonic, electrical, and nuclear magnetic resonance imaging, have been developed and applied to study complex multiphase phenomena (Rowe, 1971; Seville et al., 1986; Beck and Williams, 1996; Kumar et al., 1997; Warsito et al., 1999; George et al., 2000). Electrical capacitance tomography (ECT) is one of a handful of real-time tomography techniques and has been recently applied to three-phase flow imaging using a new image reconstruction technique (Warsito and Fan, 2001a). ECT has also been applied to other solid flow systems including standpipe flow, circulating fluidized beds, pneumatic conveying, and cyclone diplegs (Dyakowski et al., 1997, 2000; Yang and Liu, 2000; Malcus and Pugsley, 2001; Smolders et al., 2001). However, little is reported on the imaging of the turbulent fluidized beds.

Many commercial fluidized beds are operated in the turbulent fluidization regime at high temperatures. Studies of the turbulent regime have indicated the effect of temperature on the transition velocity from the bubbling to the turbulent regimes U_c, bubble size, and bubble rising velocity (Cai et al., 1989). The effect of temperature on global and local nonhomogeneity of bed properties such as bubble fraction and solids holdup in the bubble/void and the emulsion phases remains unclear. The addition of a small amount of fine particles to a bed of fluidized coarse particles is known to yield a significant effect on the reactant conversion in a turbulent fluidized bed when used as a reactor. The fundamental understanding of the role that fines play in determining the transport properties of the bed such as solids mixing and heat transfer is an important research goal. Sun and Grace (1990) studied the effect of particle-size distributions on the performance of a catalytic fluidized-bed reactor and the wide size distribution yielded the highest reactant conversion. Recent studies in this group on the effect of fines addition on gas and solids mixing also indicate that a 10–20% fines addition produces a significant enhancement of the mixing behavior (Du et al., 2002).

The specific objective of this study is to characterize the dynamic behavior of the emulsion phase and bubble/void phase properties in the turbulent fluidized bed using the optical fiber probe and electrical capacitance tomography (ECT) based on a newly developed image reconstruction technique. The effects of temperature and fines addition on the dynamic behavior of turbulent fluidization are also investigated.

Experimental Studies

Experimental setup

Two fluidized-bed units are used in this study. One bed is a stainless steel fluidized bed of 0.203 m I.D. and 2.5 m in height, which can be operated at high temperatures up to 435°C and elevated pressures up to 3.5 atm. A sintered stainless steel sheet with a pore size of 20 μm and a fractional free area of 60% is employed as a distributor. The second bed used is a plexiglas fluidized bed of 0.1 m I.D. and 1.9 m in height with a porous plate distributor with the same pore size and fractional free area as that of the stainless steel column. A two-stage cyclone separates gas and particles and is installed in the freeboard of each fluidized bed. Details of the experimental setup have been reported elsewhere (Du et al., 2002). A differential pressure transducer is installed to measure the pressure drop and the overall voidage of the fluidized bed. The fluidized particles are FCC catalyst with a mean diameter of 60 μm and particle density of 1,400 kg/m^3. The fine particles used are FCC catalyst with a mean diameter of 25 μm and particle density of 1,400 kg/m^3. They are fluidized with air. The superficial gas velocity is varied from 0.2 to 1.0 m/s, covering both the bubbling and the turbulent fluidization regimes.

ECT

The ECT system consists of a capacitance sensor, data acquisition system, and computer system for image reconstruction, interpretation, and display. Figure 1 shows the 0.1-m fluidized bed where the ECT system is applied in the experiments. The capacitance sensor array consists of a twin-plane sensor (plane 1 and plane 2) using 12 electrodes for each plane attached to the outside of the column wall. The length of each electrode is 0.05 m. Planes 1 and 2 are 0.15 m and 0.2 m above the distributor, respectively. Two 0.05-m-long guard sensor planes are located below and above the measuring sensor planes to adjust the electrical field within the sensoring area. The static bed height is 0.35 m. There are 66 combi-

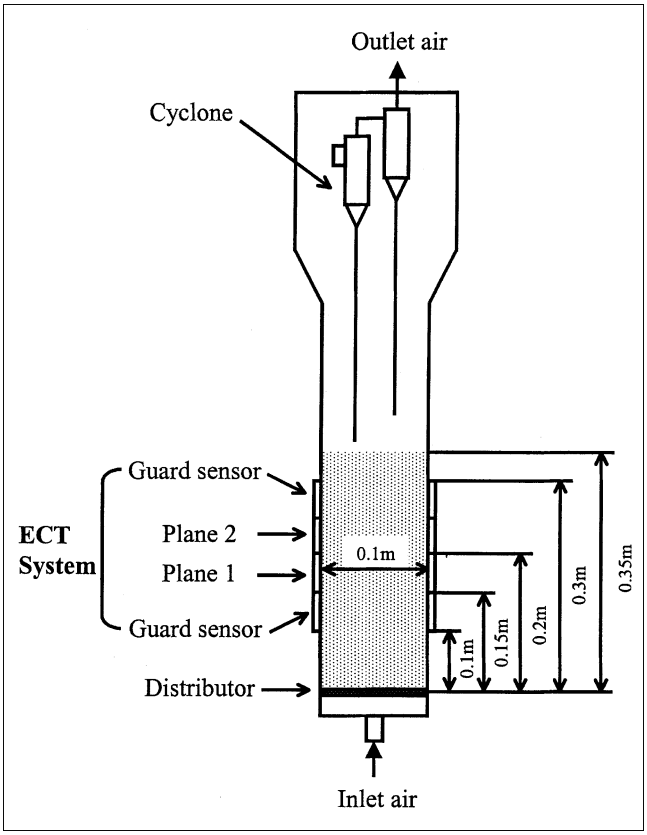

Figure 1. Fluidized bed mounted with the ECT system.

nations of independent capacitance measurements between electrode pairs from 12 electrodes. The data acquisition system manufactured by Process Tomography Limited (U.K.) is employed for capturing the ECT images at 100 frames per second. The image reconstruction is achieved using a new reconstruction algorithm based on an analog neural network multicriteria optimization image reconstruction technique (NN-MOIRT) developed earlier by the authors (Warsito and Fan, 2001b). The technique transforms capacitance data into cross-sectional images of the gas-solids two-phase flow at 32 $\times$32 pixels per image. This reconstruction technique is based on optimization of the multicriteria objective functions including: (a) the entropy function; (b) the least-weighted square error between the measured capacitance data set and the estimated capacitance from the reconstructed image; and (c) a smoothness function that gives a relatively small peakedness in the reconstructed image. The multicriteria optimization image reconstruction problem is then solved using modified Hopfield model dynamic neural-network computing. The reconstruction results by NN-MOIRT show its high accuracy, consistency (with respect to the shape), and robustness to the existing noise well over those from other available techniques, such as linear back projection (LBP) or iterative linear back projection (ILBP). Because of the unique properties of this algorithm, it can be applied to study the local dynamic behavior of complex two-phase or three-phase media with confidence. The details on this technique, the image reconstruction algorithm, and its comparisons with other algorithms, are described elsewhere (Warsito and Fan, 2001b).

Optical fiber density probe

A 3 mm I.D. optical fiber density probe consists of two parts of silver quartz fibers, one for light emitting and the other for light receiving, as shown in Figure 2. The light from the light source is introduced into the bed through the light emitting fibers and the light reflected in front of the probe is then captured by the receiving fibers. Both the reflected and the incident light are transferred to the photomultipliers where the voltage signals based on the light intensity are generated. The ratio of intensities between reflected light and light source is used as the output signal for the density measurement, which can eliminate the influence of light source variation on the measurement results. The probe can move along the axial and radial directions so that the solids concentration profile in the bed can be obtained. For each run, the data acquisition frequency is set at 400 Hz for a period of 20 s.

The relationship between the output signals of the optical fiber probe and the solids concentration in the measurement volume is nonlinear (Lin et al., 2001). Therefore, a reliable calibration is necessary to ensure an accurate measurement. In this study, based on the axisymmetry assumption, the cross-sectional time-averaged output signal N can be obtained by integrating the time-averaged output signals at different radial positions Nr, over the whole cross section

$$N = \frac{\Sigma N_r A_r}{\Sigma A_r} \tag{1}$$

The calibration process is then performed by relating the output signal N to the cross-sectional solids concentration calculated by the pressure drop measured by the differential pressure transducer.

Approaches

ECT

To verify the ECT technique in measuring the flow behavior in a gas-solid fluidized bed, the tomographic images of bubbles in a gas-solid fluidized bed are obtained under well-established conditions, as shown in Figure 3. Glass beads with

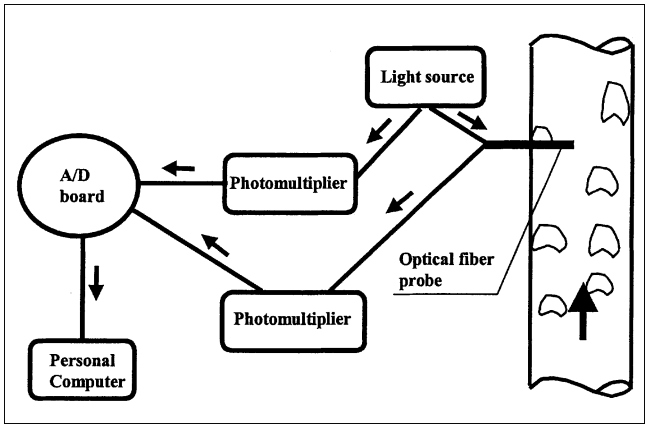

Figure 2. Optical fiber density probe.

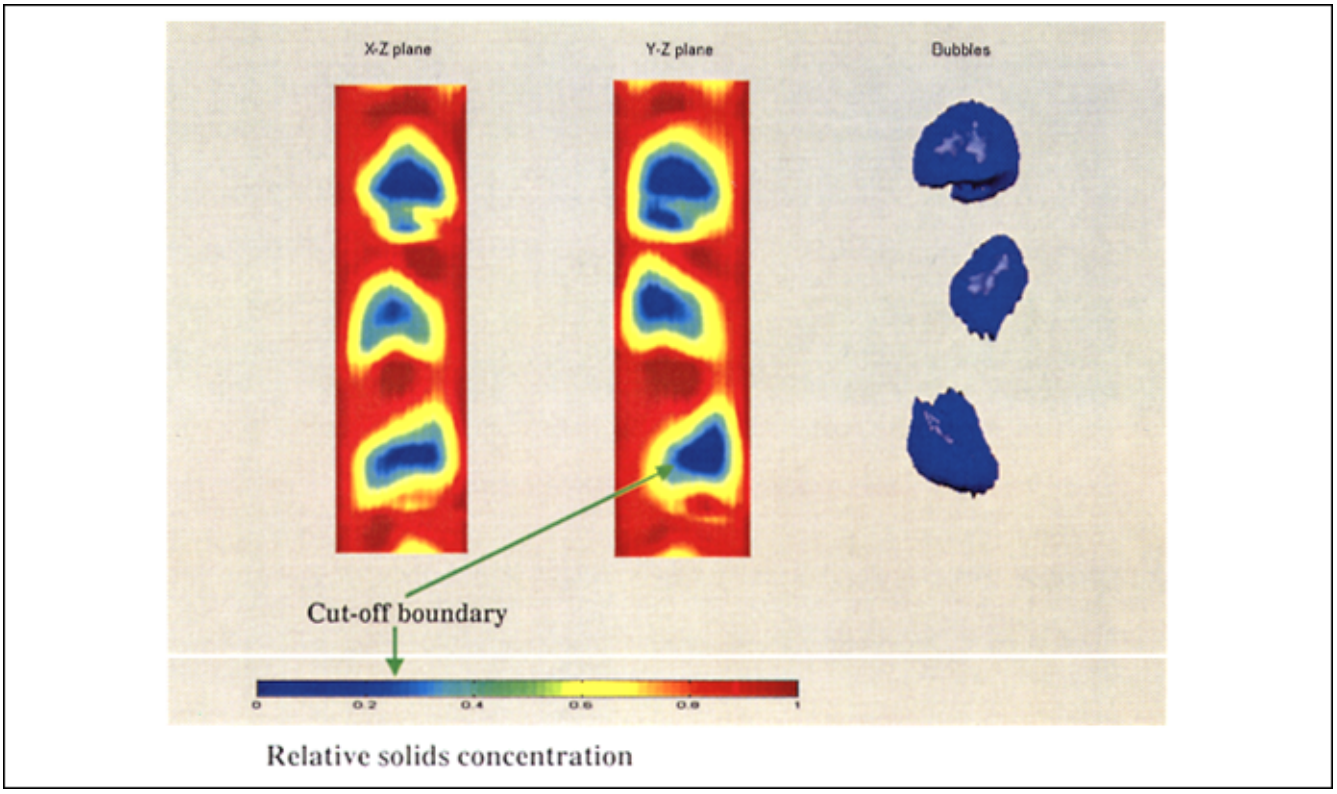

Figure 3. Bubbles in a gas-solid fluidized bed with 200 μm glass beads.

$U_g = 0.20$ m/s.

a diameter of 200 μm and a density of 2,500 kg/m^3 are fluidized by air at a superficial gas velocity of 0.2 m/s. The static bed height is set at 0.35 m. The color bar shows the relative solids concentration, spanning from zero (blue) to one (red). Zero is set for the empty bed and one is set for the packed bed. The solids concentration in a packed bed $\epsilon_{s,p}$, can be calculated from the gas density ρ_g, particle density ρ_s, and the bulk density ρ_b, as follows

$$\epsilon_{s,p} = \frac{\rho_b - \rho_g}{\rho_s - \rho_g} \tag{2}$$

The solids concentration ϵ_s can be obtained by multiplying the relative solids concentration with $\epsilon_{s,p}$. It is observed that bubbles (blue area) are generally of spherical cap or ellipsoidal cap shape. The yellow color zone surrounding the bubble represents the cloud region, similar to that reported earlier by Rowe (1971) using the X-ray method. The bubble wake, bubble drift pattern, and wake shedding are also observed as the dark red color behind the bubble in the figure. There are numerous published equations predicting the bubble size in fluidized beds. Table 1 provides the predictive results on the bubble size based on several commonly used equations including those of Rowe (1976), Werther (1976), Darton et al. (1977), and Cai et al. (1994). The results are comparable to the value of 50 mm estimated directly from Figure 3. The existence of the cloud can also be verified by comparing the rise velocity of single bubbles U_{br} and upward velocity of gas at minimum fluidization $U_f (= U_{mf}/\epsilon_{mf})$. U_f can be calculated from the Ergun equation under the minimum fluidization condition. U_{br} is determined by the following equation of Kunii and Levenspiel (1991)

$$U_{br} = \left[0.711(gd_b)^{1/2}\right] \times 1.2 \exp\left(-1.49\frac{d_b}{d_t}\right), \; 0.125 < \frac{d_b}{d_t} < 0.6 \tag{3}$$

Under this experimental condition, the calculated result of U_{br} is much larger than that of U_f, which indicates the exist-

Table 1. Commonly Used Equations for Estimating Bubble Size in Fluidized Beds

Author	Equation	Result (m)
Rowe (1976)	$d_b = (U - U_{mf})^{0.5} h^{0.75}/g^{0.25}$	0.068
Werther (1976)	$d_b = 0.00853[1 + 27.2(U - U_{mf})]^{1/3}(1 + 6.84h)^{1.21}$	0.043
Darton et al. (1977)	$d_b = 0.54(U - U_{mf})^{0.4} h^{0.8}/g^{0.2}$	0.046
Cai et al. (1994)	$d_b = 0.38h^{0.8}(U - U_{mf})^{0.42}$ $\exp[-1.4 \times 10^{-4} - 0.25(U - U_{mf})^2 - 0.1(U - U_{mf})]$	0.048

ence of the cloud around the bubble (Davidson, 1961). Based on the results of U_{br} and U_f, the radius of cloud surrounding a bubble R_c can be determined as follows (Davidson, 1961)

$$\frac{R_c^3}{R_b^3} = \frac{U_{br} + 2U_f}{U_{br} - U_f} \tag{4}$$

The calculated value of R_c is about 31 mm and thus the thickness of the cloud is about 7 mm, which is also in good agreement with that estimated from Figure 3, that is, 8 mm. As the distance between the imaging planes 1 and 2 is 5 cm, the bubble velocity can be estimated from the bubble tracking time between these two planes. The bubble rise velocity in Figure 3 is estimated to be 35 cm/s, which is again comparable to the value calculated by Eq. 3, that is, 30 cm/s. These three verifications, bubble size, cloud size, and bubble velocity, demonstrate the accuracy of the image reconstruction technique employed for the ECT for the gas-solid fluidization study.

Determination of the bubble/void phase based on the ECT measurement

To determine the dynamic behavior of both the bubble/void phase and the emulsion phase in a fluidized bed, the phase boundary between the bubble/void phase and emulsion phase needs to be identified. Two methods, based on a two-region model and a direct image calculation, are developed for this purpose. Figure 4 shows the relative relationship between the tomography and the two-region model. The lower part of the figure indicates the field information. L_0 is the length of the ECT electrode, that is, 5 cm. L_b represents the length of a bubble in the measuring volume. The white area is the bubble. The bed comprises two regions: Region A is the area including both the emulsion phase and the bubble/void phase. Region B indicates the area where almost no bubble/void phase exists. The upper part of the figure shows the tomographic image averaging over the 5 cm length of the measurement area in the lower part. It is clear that region A corresponds to the white area and region B corresponds to the gray area in the tomogram. Thus, the two-region model is proposed based on the following two assumptions:

(1) The solids holdup in the emulsion phase in region B is the same as that in region A.

(2) The solids holdup in the bubble/void phase is negligible compared to that in the emulsion phase.

The bubble/void phase fraction δ_b can then be calculated from the overall solids holdup, according to

$$\begin{aligned} \delta_b &= 1 - \delta_e \\ \epsilon_s &= \epsilon_{es}\delta_e + \epsilon_{bs}\delta_b \\ \epsilon_{bs} &\approx 0 \end{aligned} \tag{5}$$

The bubble/void phase fraction can also be calculated directly from the quasi-3D image by means of setting the boundary of the solids holdup value for the bubble phase (direct image calculation), as shown in Figure 3. In this work, the cut-off boundary is set at a relative solids holdup of 0.25 and the size and shape of bubbles are shown in the third column of Figure 3.

Comparisons between the ECT measurement and the optical fiber probe measurement

Figure 5 shows the comparison of the time-averaged solids holdup profiles at different radial positions measured by the ECT and the optical fiber probe in a 0.1 m I.D. fluidized bed. In the center of the bed, the solids holdup measured by the optical fiber is larger than that measured by the ECT. The

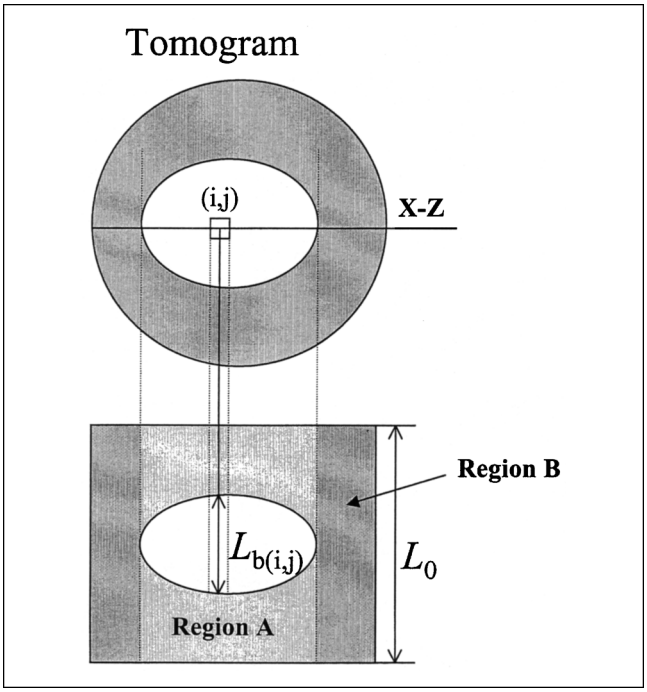

Figure 4. Determination of the bubble/void phase fraction based on the two-region model in the ECT measurement.

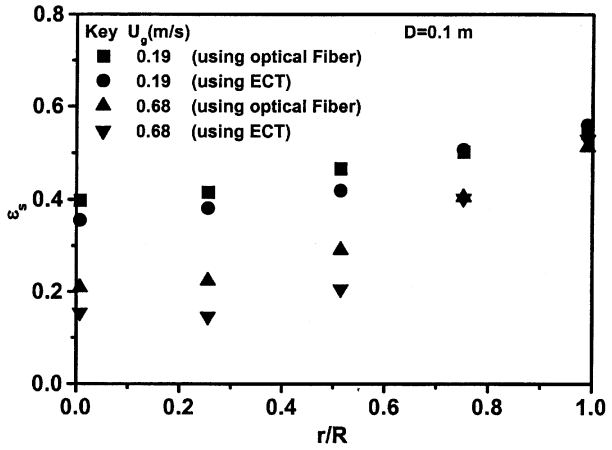

Figure 5. Comparison of time-averaged solids holdup profiles measured by the ECT and the optical fiber probe.

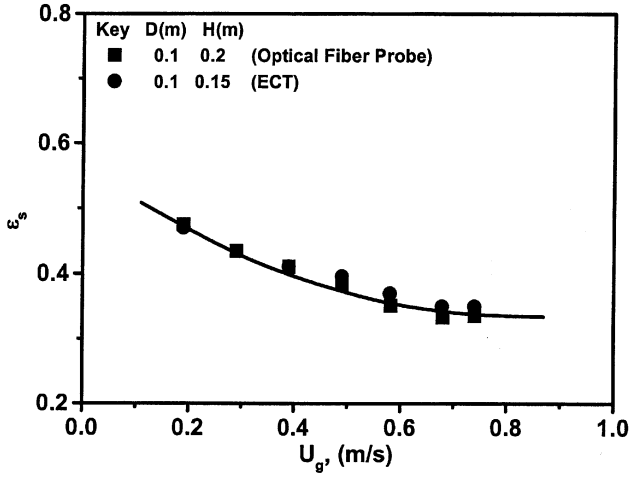

Figure 6. Variation of time-averaged cross-sectional solids holdup with gas velocity.

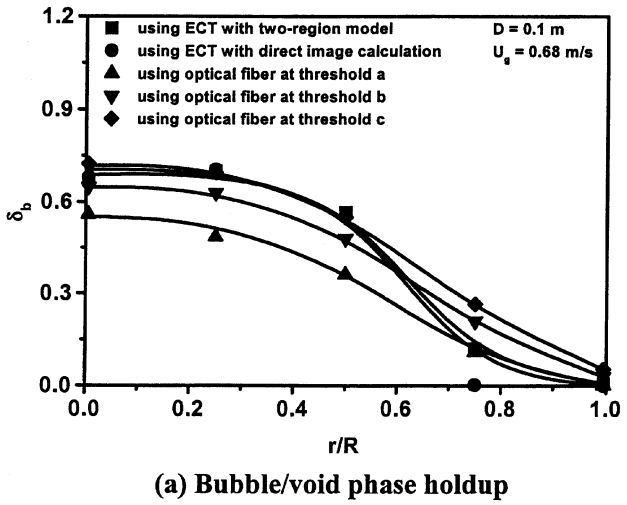

(a) Bubble/void phase holdup

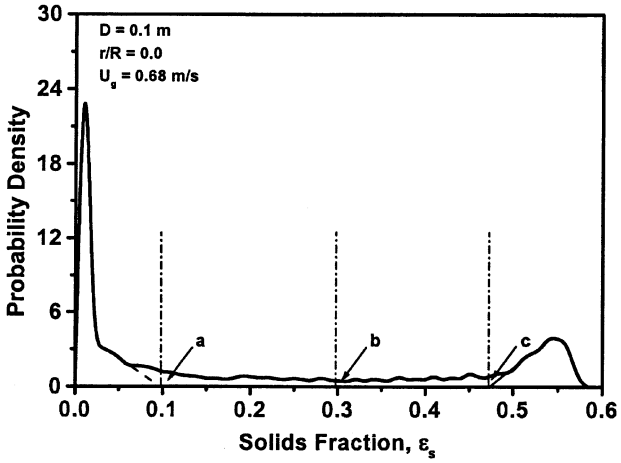

(b) Selection of threshold

Figure 7. Effect of threshold selection on the determination of the bubble/void phase fraction.

difference between these two techniques is larger at higher gas velocities. In the wall region, on the other hand, the solids holdup measured by the optical fiber is slightly lower. It is known that the bubble phase is dominantly present in the core region of the bed and the solids holdup in the bubble phase is very low. When an optical fiber probe is placed in a bubble, the solids holdup measured reflects not only the solids holdup but also the dense solids surrounding the bubble phase and, hence, higher overall solids holdup in the core region. With the increase of the gas velocity, the bubble phase fraction increases and the light-reflection effect of the solid particles in the bubble phase increases, and, hence, there is a higher measurement difference of the optical fiber probe at higher gas velocities. In the wall region, the slight reduction of the solids holdup obtained by the optical fiber probe can be attributed to the minimal effect of the bubble phase and the interference of the probe with the flow behavior in this region. Although the time-averaged solids holdup at different radial positions are somewhat different, the time-averaged cross-sectional solids holdup measured by the ECT is comparable to that measured by the optical fiber probe, as shown in Figure 6. The difference between both techniques for the solids holdup in the core region does not significantly alter the overall solids holdup in a bed cross-section.

For the measurement of the local bubble/void phase fraction δ_b, two peaks, one detecting the bubble/void phase and the other the emulsion phase, are present in the probability density function (PDF) curves of the local solids fraction signals. To identify each of these two phases from the signals, a threshold value needs to be set. Bi and Su (2001) selected two thresholds: one between the two peaks and the other at the peak of the lower solids holdup in the PDF curve. Lin et al. (2001) used a combined PDF to describe the probability density distribution (PDD) of the transient signals of the solids fraction. The threshold ϵ_{sm} to distinguish the two phases was set as follows

$$\epsilon_{sm} = \overline{\epsilon_{sc}} - 3\sigma_c, \tag{6}$$

Cui et al. (2000) selected the local voidage point with the minimum probability density between the two peaks in the PDF curves as the threshold to identify the bubble/void phase and the emulsion phase. According to the threshold value, the bubble/void phase fraction can be obtained by the ratio of the area below this value and the total area underneath the PDF curve.

To illustrate the effect of the threshold value on the determination of the bubble/void phase, three typical thresholds, that is, point ***a*** on the left side, ***b*** in the middle, and ***c*** on the right side in the PDF curve of the local transient solids fraction signals obtained by the optical fiber probe, are selected, as shown in Figure 7b. The bubble/void phase fraction at different radial positions in the bed at a gas velocity of 0.68 m/s obtained by these three thresholds are compared with those calculated by the two-region model and the direct image calculation based on the ECT measurement, as shown in Figure 7a. It is seen that the bubble phase fraction obtained by different threshold values varies significantly, which is similar to the results obtained by Bi and Su (2001). The bubble/void phase fraction obtained by the ECT with the two-region model and the direct image calculation are almost

the same both in the core region and in the wall region, which further demonstrates the reliability of the ECT technique applied to the measurement of dynamic behavior in a gas-solid fluidized bed. Compared with the results obtained by the ECT, the optical fiber probe based on threshold ***c*** yields almost the same results in the core region, but overestimates results in the wall region. On the other hand, the optical fiber probe based on threshold ***a*** shows underestimation in the core region and similarity in the wall region, while probe data based on threshold ***b*** shows significant deviation both in the core and in the wall region. Thus, to be accurate, a combined threshold selection based on threshold ***a*** for the wall region and threshold ***c*** for the core region can be best utilized to represent the bubble/void phase fraction in a gas-solid fluidized bed.

Results and Discussion

Dynamic behavior in the bed

For this small-diameter column of 0.1 m ID used in this experiment, slugging could occur. Based on the criterion given by Baeyens and Geldart (1974), the minimum bed height for slugging is 0.9 m. In this work, to ensure no slug is present in the column, the static bed height is set at 0.35 m. The visual observation also reveals that there is no slug for these 60 μm FCC particles during the experiments.

The solids holdup distributions with and without fines addition in real time (with a time interval of 0.02 s) in planes 1 and 2 in the bubbling regime at a gas velocity of 0.19 m/s and in the turbulent regime at a gas velocity of 0.74 m/s are shown in Figures 8 and 9, respectively. The blue area representing the low solids concentration indicates the presence of the bubble/void phase. The red area is for the emulsion phase with a high solids concentration. In both the bubbling and the turbulent regimes, it is seen that bubble/void phase undergoes temporal and phase fraction variation. Some light yellow areas exist in the bubble/void phase (blue areas) especially in Figure 9. By comparing the solids holdup distribution in plane 1 and plane 2, it can be seen that the distribution patterns in the plane pairs are quite similar and bubbles in plane 1 are slightly smaller than those in plane 2. This indicates that the bubbles/voids in the lower plane (plane 1) move into the upper plane (plane 2) while growing. The effect of 10% fines addition on the real time solids holdup distribution is also shown in the figure. The breakup of large bubbles to small ones is clearly indicated for both the bubbling and the turbulent regimes.

Figure 10a shows the 20-s time-averaged cross-sectional solids holdup distribution at different gas velocities in planes 1 and 2. At high gas velocities, especially in the turbulent regime, the time-averaged cross-sectional solids holdup exhibits a radial symmetric distribution, while this is not the case for the bubbling regime. The results substantiate the validity of the axisymmetry assumption for the turbulent regime in the optical fiber probe measurement of solids holdups in the bed as stated earlier. At low gas velocities in the bubbling regime, dispersed bubbles yield a lower solids concentration in the center of the bed (light blue areas). The asymmetric distribution of solids concentration is due to the spiral motion of bubbles in the bed. However, in the turbulent regime, the blue areas in the core region and the red and yellow areas in the wall region exhibit the alternating nature of the bubble/void phase and the emulsion phase for being the continuous phase. The axisymmetric distribution of solids concentration can be attributed to the movement of numerous small voids in the bed. Figure 10b indicates the time-averaged cross-sectional solids holdup distribution with 10% fines addition. Although the bubble breakup occurs with different instantaneous bed behavior compared to without fine particles, the time-averaged cross-sectional solids holdup distribution is almost unchanged with the addition of 10% fine particles.

By stacking 200 tomographic images obtained in 4 s from the same plane, a quasi-three-dimensional (3-D) flow structure of the gas-solid fluidized bed can be displayed and is shown in Figure 11. The vertical coordinate, Z-coordinate, represents "time" with the length scale for the time coordinate taken as the bubble rise velocity multiplying the time. The bubble rise velocity is obtained through the cross-correlation of the gas holdup distributions in two reference planes. The images from two sliced sections representing the 3-D solids holdup distribution in the X-Z and Y-Z planes are shown in the figures along with the quasi-3-D bubble flow. The distinction of bubble or bubble/void phase from the emulsion phase is made through direct image calculation discussed in the following section. It is seen that the bubble rises spirally and rocks between the sides of the column wall. Du et al. (2002) showed a similar flow structure in a bubbling bed. The significant effect of fines addition on the flow structure, especially on the bubble behavior, is given in this figure. More particles, especially fine particles, may exist at the center of the bed moving through the bubbles, resulting in the breakup of large bubbles into small bubbles or voids. With the addition of fine particles, the bubble shape becomes more irregular.

Dynamic behavior in the bubble/void phase

Based on the ECT imaging, the dynamic characteristics of the bubble/void phase and the emulsion phase can be quantified. Figure 12a illustrates the fluctuations of the cross-sectional averaged bubble/void phase fraction at different gas velocities covering the bubbling, the transition, and the turbulent regimes. The dynamic behavior without fines addition is compared to 10% fines addition for the three gas velocities $U_g = 0.19$, 0.49, and 0.87 m/s. At a lower gas velocity of 0.19 m/s in the bubbling regime, the magnitude of the fluctuations is low, reflecting the effect of small bubbles. There are many moments when the bubble phase fraction is nearly zero reflecting the low gas holdups in bubbling fluidization. As the gas velocity increases in the transition regime ($U_g = 0.49$ m/s), the magnitude of the fluctuations increases, indicating bubble growth. The large peaks indicate a large bubble has gone past the sensor. The smaller magnitude, higher frequency peaks indicate a series of small bubbles going past the sensor. The presence of both these types in the $U_g = 0.49$ m/s plots is evidence of large and small bubbles coexistence, which is typical of bubble coalescence and breakup. It is consistent with the transition mechanism depicted by Cai et al. (1989).

With a further increase of the gas velocity to $U_g = 0.87$ m/s, that is, well within the turbulent regime, the magnitude and the frequency of the fluctuations all decrease slightly. It indi-

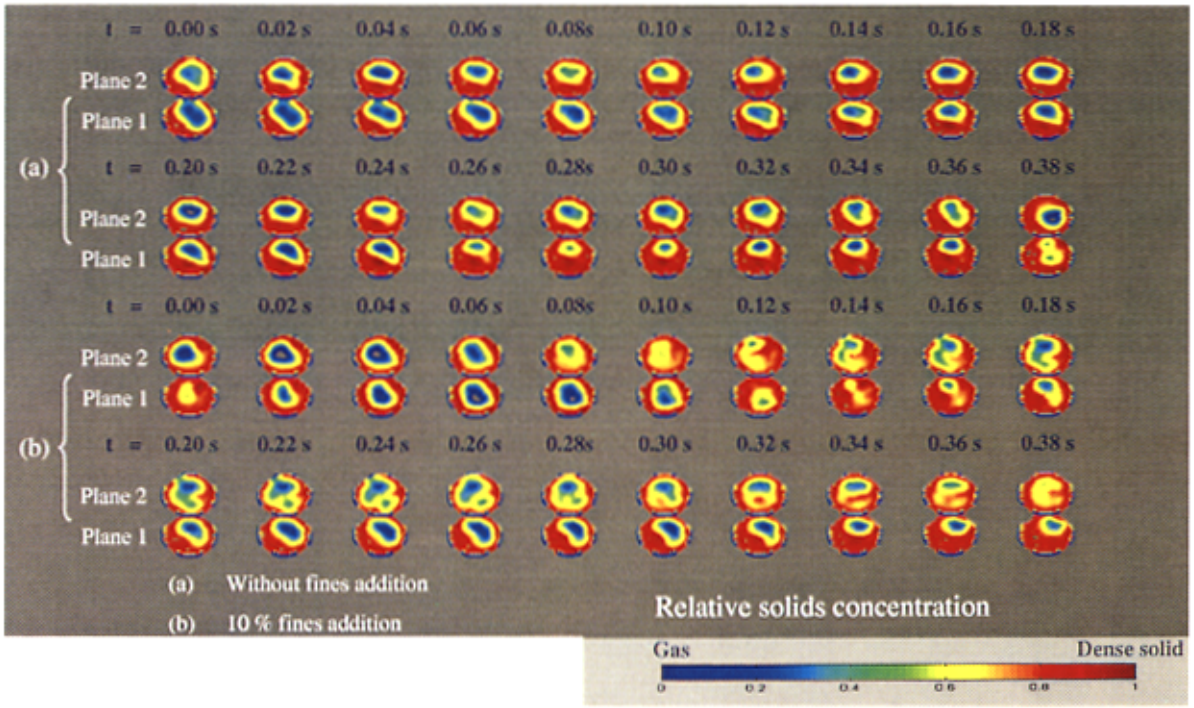

Figure 8. Real-time solids holdup distributions at a gas velocity of 0.19 m/s.

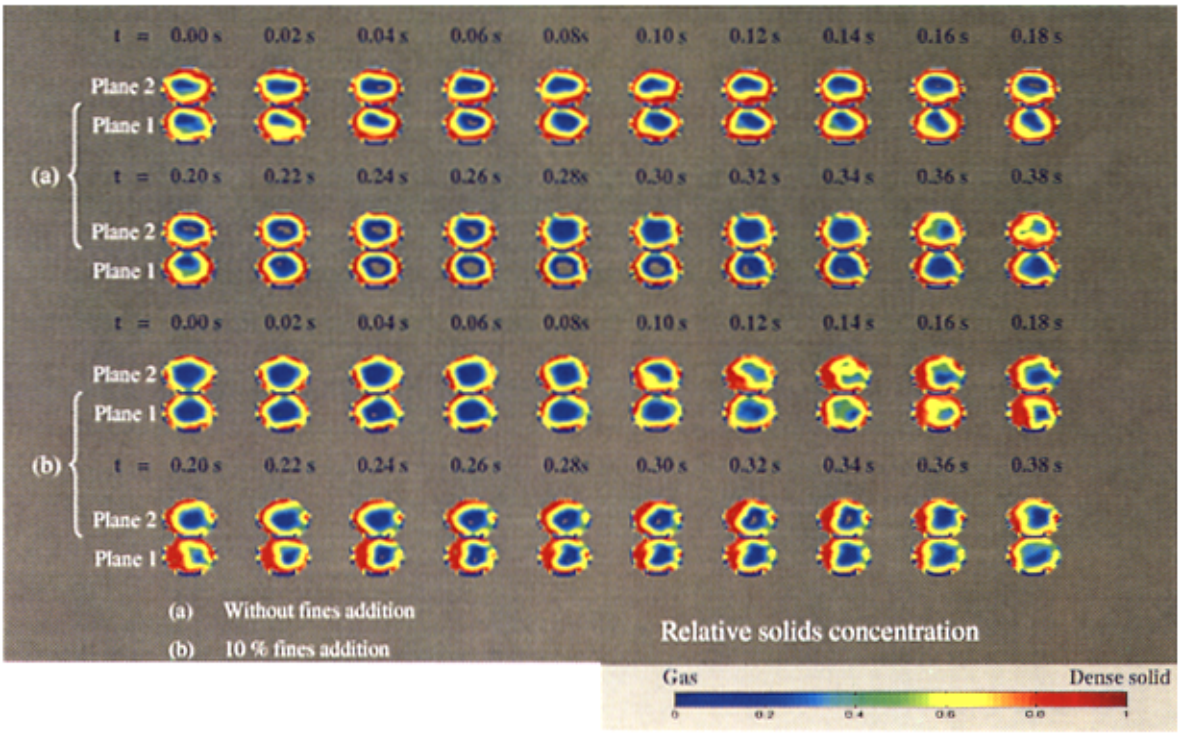

Figure 9. Real-time solids holdup distributions at a gas velocity of 0.74 m/s.

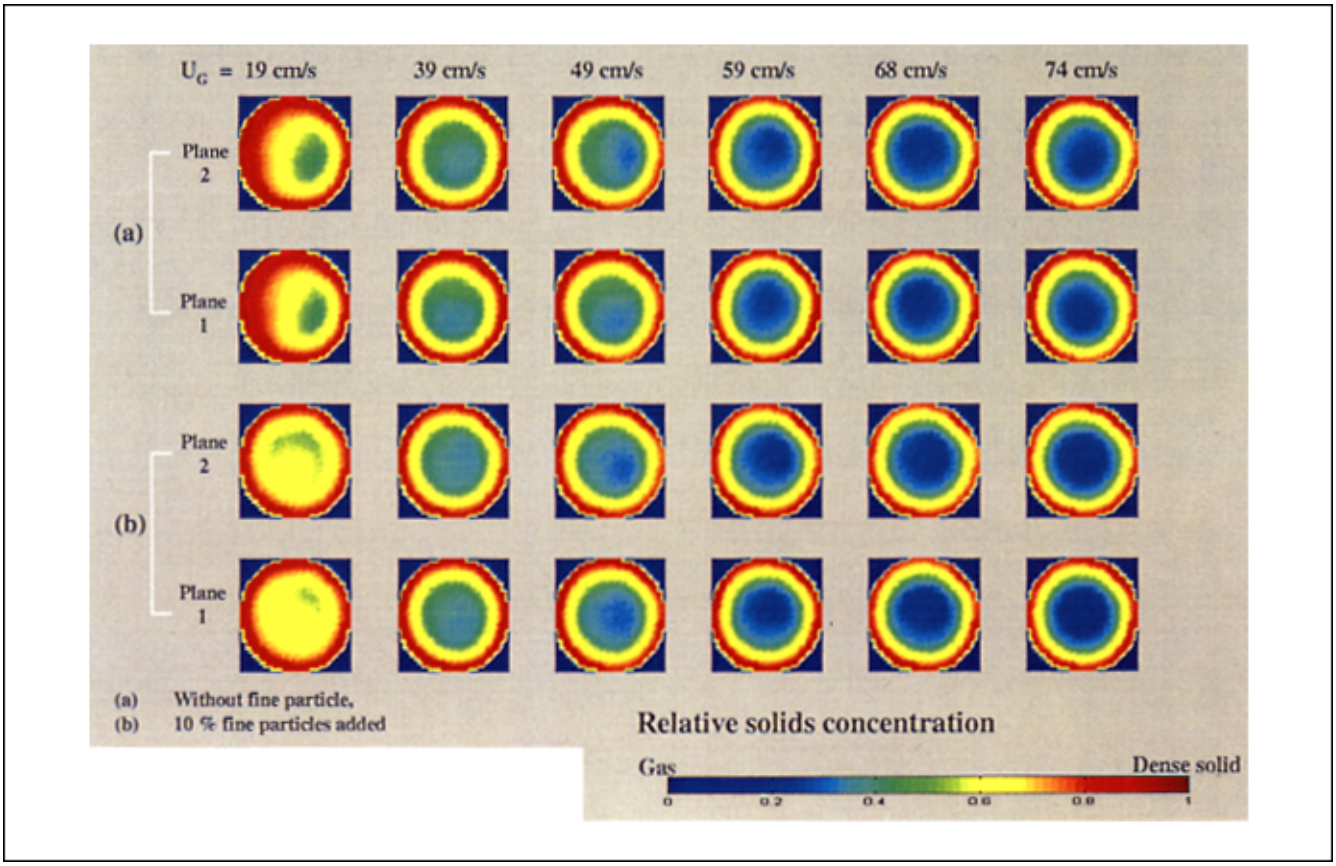

Figure 10. Time-averaged cross-sectional solids holdup distributions.

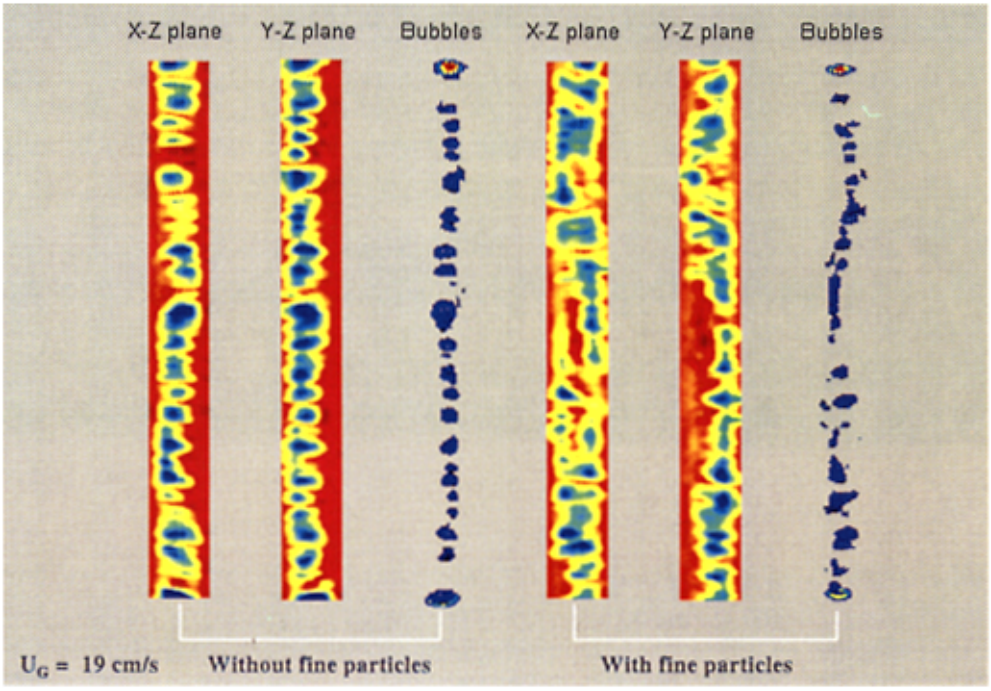

Figure 11. Quasi-3D flow structures of a gas-solid fluidized bed at a gas velocity of 0.19 m/s.

cates that the fluidization quality in the turbulent regime is enhanced compared to the bubbling regime. Notice that there still are few moments of zero or near zero values of bubble/void phase fraction. This brings up again the alternating nature of the bubble/void phase and the emulsion phase behaving as the continuous phase in the bed in the turbulent regime as reported by Bi et al. (2000). With a 10% fines addition, the magnitude of the fluctuation decreases in the bubbling and the turbulent regimes and varies slightly in the transition regime. The bubbles or voids disintegrate into small bubbles or voids with fines addition, allowing smooth bubble flow and, hence, decreasing the fluctuation of the bubble/void phase fraction. However, in the transition regime, the bed is in the state of concurrent bubble breakup and coalescence, resulting in a small effect of fine particles on the bubble dynamics.

To relate the fluctuations of the bubble/void phase fraction to the local flow structure, the corresponding power spectral analyses are carried out as shown in Figure 12b. A continuous broad power spectrum with low dominant frequency is obtained for both the bubbling and the turbulent regimes, which is consistent with the results of Chehbouni et

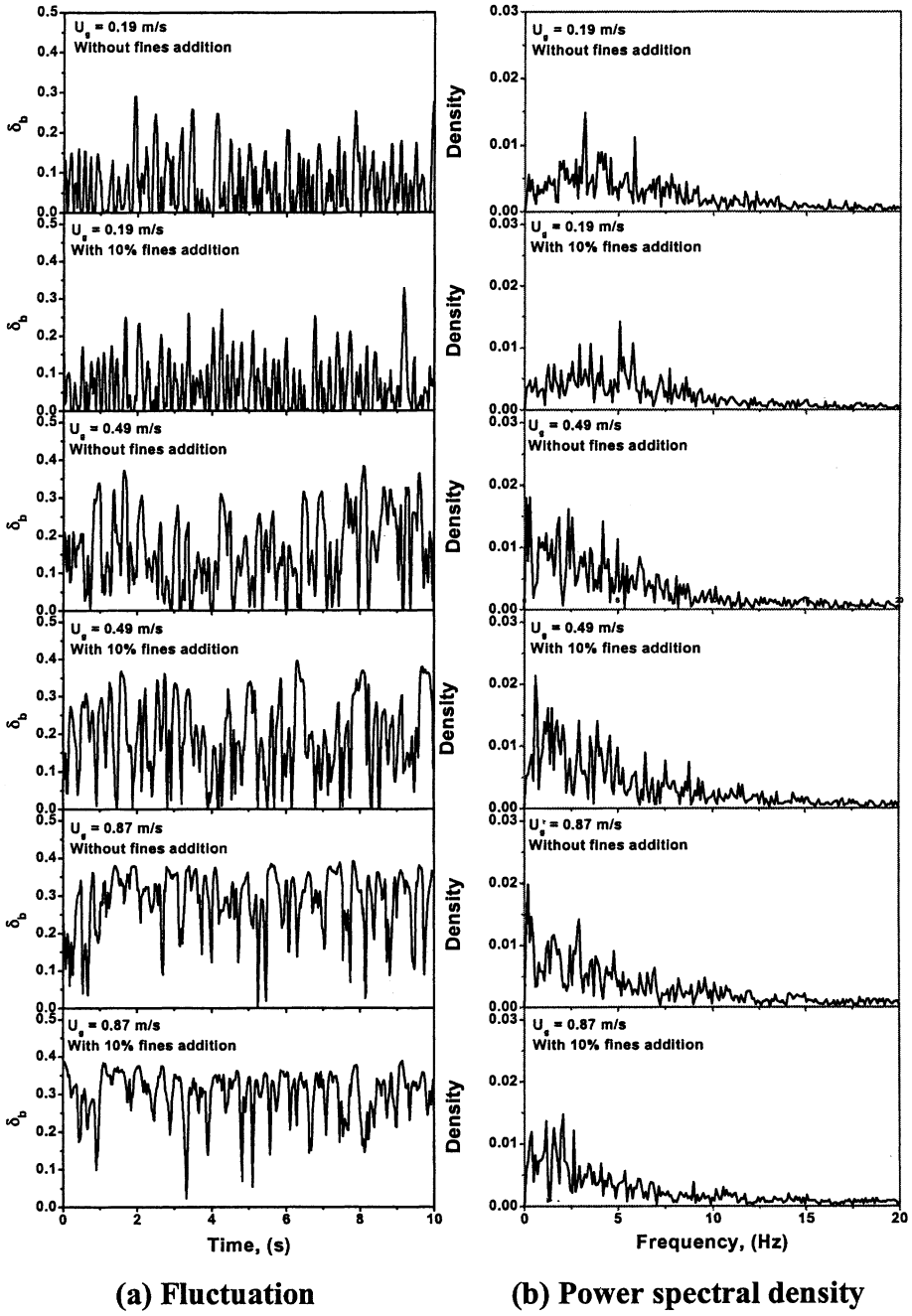

Figure 12. Fluctuations of cross-sectional averaged bubble/void phase fraction and their corresponding power spectral densities.

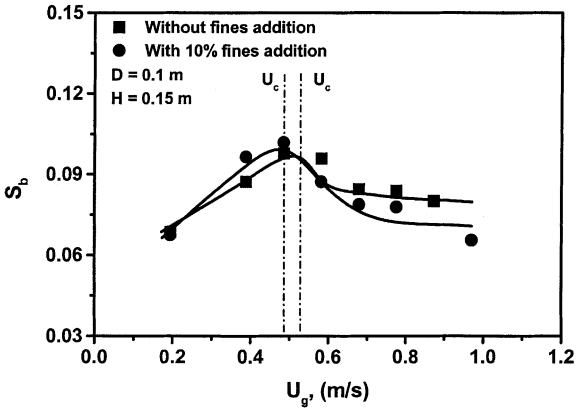

Figure 13. Standard deviation of the cross-sectional averaged bubble/void phase fraction fluctuation.

al. (1994) using a capacitance probe and of Bai et al. (1999) using an optical fiber probe. In the bubbling regime, the dominant frequency is about 3 Hz. With an increase in the gas velocity in the transition regime, the dominant frequency decreases to 2 Hz, while the spectral energy increases. In the turbulent regime, the dominant frequency decreases to 1.5 Hz, while the spectral energy further increases. This can be attributed to the turbulent movement of small voids in the bed. At the same gas velocity, the spectral energy decreases with fines addition in the bubbling and turbulent regimes, indicating that the fines addition enhances the fluidization quality. The dominant frequency remains almost unchanged with fines addition. The dominant frequencies obtained in this work are all higher than those obtained by Bai et al. (1999). This may be explained by fact that the fluctuation signals obtained by Bai et al. (1999) were of the local bed voidage that includes the gas holdups in both the bubble/void phase and the emulsion phase.

Figure 13 shows the standard deviation of the cross-sectional averaged bubble/void phase fraction fluctuation without fines addition and with 10% fines addition as they are varied with gas velocity. With increasing gas velocity, the standard deviation increases in the bubbling regime, peaks at the transition velocity U_c, and then decreases and levels off in the turbulent regime. The transition velocity obtained by the ECT is in agreement with that obtained by the pressure fluctuation measurement and that calculated by the correlation of Cai et al. (1989). From the ECT results, the addition of fines yields a shift in the transition velocity into the lower gas velocity range. It can be attributed to the enhanced breakup of the large bubbles into small voids due to the addition of fine particles. Although the bubble/void phase fraction increases in the turbulent regime, the magnitude of the fluctuation decreases due to the smaller sizes of the voids. This finding further illustrates the physical significance of the transition velocity U_c.

Figure 14 shows the typical radial distribution of the time-averaged bubble/void phase fraction obtained by the ECT with the two-region model and the optical fiber probe with the combined threshold method at a gas velocity of 0.68 m/s. For reference, results from the literature are also plotted. As can be seen, the results match reasonably well, indicating that the combined threshold method is a feasible way to determine the bubble/void phase in gas-solid fluidization for the local probe measurement. From the profile, it is clear that the bubble/void phase tends to be concentrated in the core region. The reported bubble/void phase fraction profiles (Nakajima et al., 1991; Bayle et al., 2001; Lin et al., 2001), along the radial positions measured by the optical fiber probe, are much flatter than the results obtained in this work. The difference can be explained in part by the limitation of the probe measurement stated above and by the large size of beds used in the cited literature.

The time-averaged cross-sectional bubble/void phase fraction vs. the gas velocity is shown in Figure 15. The bubble/void

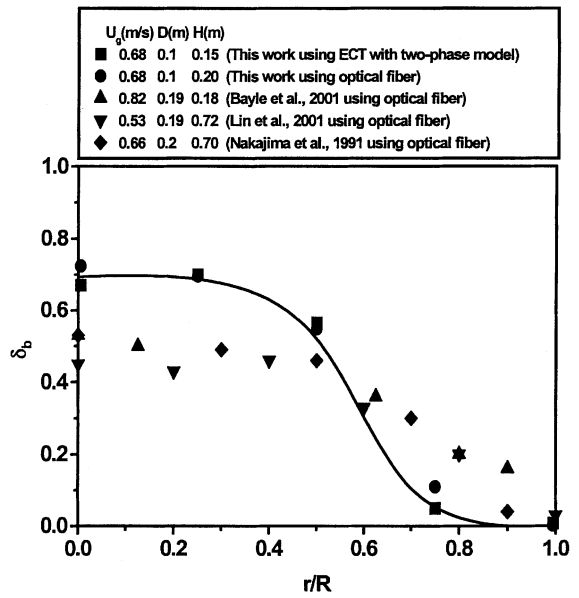

Figure 14. Typical radial distribution of the time-averaged bubble/void phase fraction.

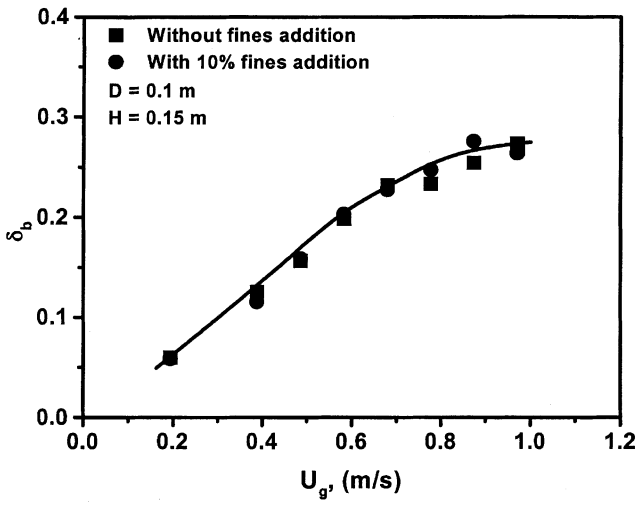

Figure 15. Variation of the cross-sectional bubble/void phase fraction with gas velocity.

phase fraction averaged over the cross section increases linearly with the gas velocity in the bubbling regime; the rate of the increase is slightly reduced in the turbulent regime. The bubble/void phase fractions remain almost unchanged with 10% fines addition, indicating that the effect of fines addition on the bubble/void phase fraction is minimal although the bubble size and shape are changed. It is known that in the turbulent regime the increasing gas velocity increases the bed voidage as a result of an increase in the bubble/void phase fraction and the gas holdup in the emulsion phase. The moderate increase of the cross-sectional bubble/void phase fraction with the gas velocity in the turbulent regime can be attributed to the fact that more gas flows through the emulsion phase. The overall bubble fraction obtained by Nakajima et al. (1991) using the optical fiber probe indicated the same bubble/void phase fraction variation behavior. By comparing the bubble fraction averaged over the bed and the total bed voidage obtained by the pressure drop, Nakajima et al. (1991) postulated that the expansion of the emulsion phase could be used to explain this moderate increase in the bubble fraction in the turbulent regime as indicated above. They used this phenomenon as a basis for defining the transition velocity from the bubbling regime to the turbulent regime U_c.

Figures 16a and 16b show the fluctuations of the solids holdup in the bubble/void phase and their corresponding power spectral densities along with the effect of fines addition. The solids holdup in the bubble/void phase is very low (less than 0.1) compared to the overall solids holdup in the bed. In the bubbling regime, the magnitude of the fluctuation increases, while the frequency decreases as the gas velocity increases. In the turbulent regime, the magnitude and the frequency of the fluctuation all decrease with the gas velocity. With 10% addition of fine particles, the magnitude of the fluctuation further decreases and the frequency increases. This indicates that the fine particles exist mostly in the bubble/void phase. Figure 16b illustrates the related power spectral densities. In the bubbling regime, the dominant frequency is about 2.5 Hz. With an increase of the gas velocity to the transition regime and the turbulent regime, the dominant frequency decreases and the spectral energy increases. At higher gas velocities, the dominant frequency is not distinct and there are some small peaks with higher frequency and lower energy (similar phenomena are also observed for the emulsion phase, which will be discussed in the following section). This may be attributed to the fact that intermittent formation and disintegration of particle clusters occur as the solids concentration in the bubble/void phase increases at increasing gas velocity. At the same gas velocity, the dominant frequency and the spectral energy all decrease with fines addition. The effect of fine particles on the small and broad peaks in the high frequency region in the power spectral density is more remarkable at higher gas velocities.

The standard deviation of the fluctuation of the cross-sectional averaged solids holdup in the bubble/void phase is shown in Figure 17. The standard deviation peaks at the transition velocity U_c. A 10% fines addition gives a lower U_c. The standard deviation with fines addition is much lower than that without fines at lower gas velocities and almost the same at higher gas velocities. It may be considered that the turbulent movement of particles induced by the bubbles is reduced with fines addition in the bubbling regime. In the turbulent regime, the combined effect of the bubble/void phase breakup and the increased particle turbulence may contribute to the slight change in the standard deviation.

The time-averaged cross-sectional solids holdup in the bubble/void phase with and without fines addition is shown in Figure 18. The solids holdup increases linearly with the gas velocity in the bubbling regime up to the transition regime and the rate of the increase then decreases in the turbulent regime. Lin et al. (2001) observed similar results, that is, an increase in the solids fraction in voids with an increase in the gas velocity based on optical fiber probe measurement. The averaged solids holdup in the bubble/void phase for the 10% fines addition is seen to be almost the same as that without fines addition, but slightly higher in the turbulent regime.

Dynamic behavior in the emulsion phase

Based on the ECT measurement, the time-series solids holdup characteristics in the emulsion phase over the cross section of the bed can be obtained. Figures 19a and 19b show the fluctuations of the cross-sectional averaged solids holdup in the emulsion phase and the corresponding power spectral densities at different gas velocities covering the bubbling, the transition, and the turbulent regimes. Compared to the magnitude of the fluctuation of the bubble/void phase fraction, the magnitude of the fluctuation of the solids holdup in the emulsion phase is relatively small. With the increase of the gas velocity to the transition regime, the magnitude of the fluctuation of the solids holdup in the emulsion phase increases due to the movement of the bubble, and the frequency decreases due to the expansion of the emulsion phase. As the gas velocity further increases, both the magnitude and the frequency decrease slightly, indicating a slight effect of the turbulent movement of small voids on the emulsion phase characteristics, especially the solids holdup distribution. The addition of 10% fine particles reduces the magnitude of the fluctuation, leading to more uniform fluidization behavior. The power spectral density properties in Figure 19b are very similar for different gas velocities. The dominant frequency is low (< 1 Hz) with high spectral energy, corresponding to the large clusters in the emulsion phase. Following the dominant frequency, there are several peaks with high frequency and low spectral energy, corresponding to the medium clusters with different sizes. Due to the limitation of the data acquisition frequency in this measurement, there might be more peaks with higher frequency and lower energy existing for different cluster sizes in the emulsion phase. The shape and the tendency of the power spectral density are similar with the fines addition. The spectral energy is shown to decrease with a lower dominant frequency as the fine particles are added in the bed. The behavior of power spectral density may reflect the fact that clusters in the emulsion phase play an important role in emulsion phase hydrodynamics. Figure 20 shows the standard deviation of the cross-sectional averaged solids holdup fluctuation in the emulsion phase against the gas velocity. The standard deviation increases in the bubbling regime, peaks at the transition velocity, U_c, and then decreases slightly and levels off in the turbulent regime. The decrease in the turbulent regime can be attributed to the expansion of the emulsion phase, which reduces the magnitude

of the solids holdup fluctuation. The standard deviation is much lower with 10% fines addition, corresponding to the decrease in the magnitude of the fluctuation shown in Figure 19a.

The time-averaged radial variation of solids holdup in the emulsion phase and the variation of time-averaged cross-sectional solids holdup in the emulsion phase with the gas velocity are shown in Figure 21a and 21b, respectively. The solids holdups in the emulsion phase in the core region are lower than those in the wall region. However, the rate of the increase from the core region to the wall region is moderate at higher gas velocities in the turbulent regime, which is similar to the results reported by Bi and Su (2001). The time-averaged cross-sectional solids holdup in the emulsion phase decreases with the gas velocity, which further substantiates the expansion of the emulsion phase in the turbulent regime, as shown in Figure 21b. Werther and Wein (1994) also reported a significant increase in dense phase voidage or a decrease in the solids holdup in the dense phase for Geldart Group B particles by analyzing the probability distributions of the local instantaneous solids volume concentrations measured by the capacitance probe. The solids concentration in the dense

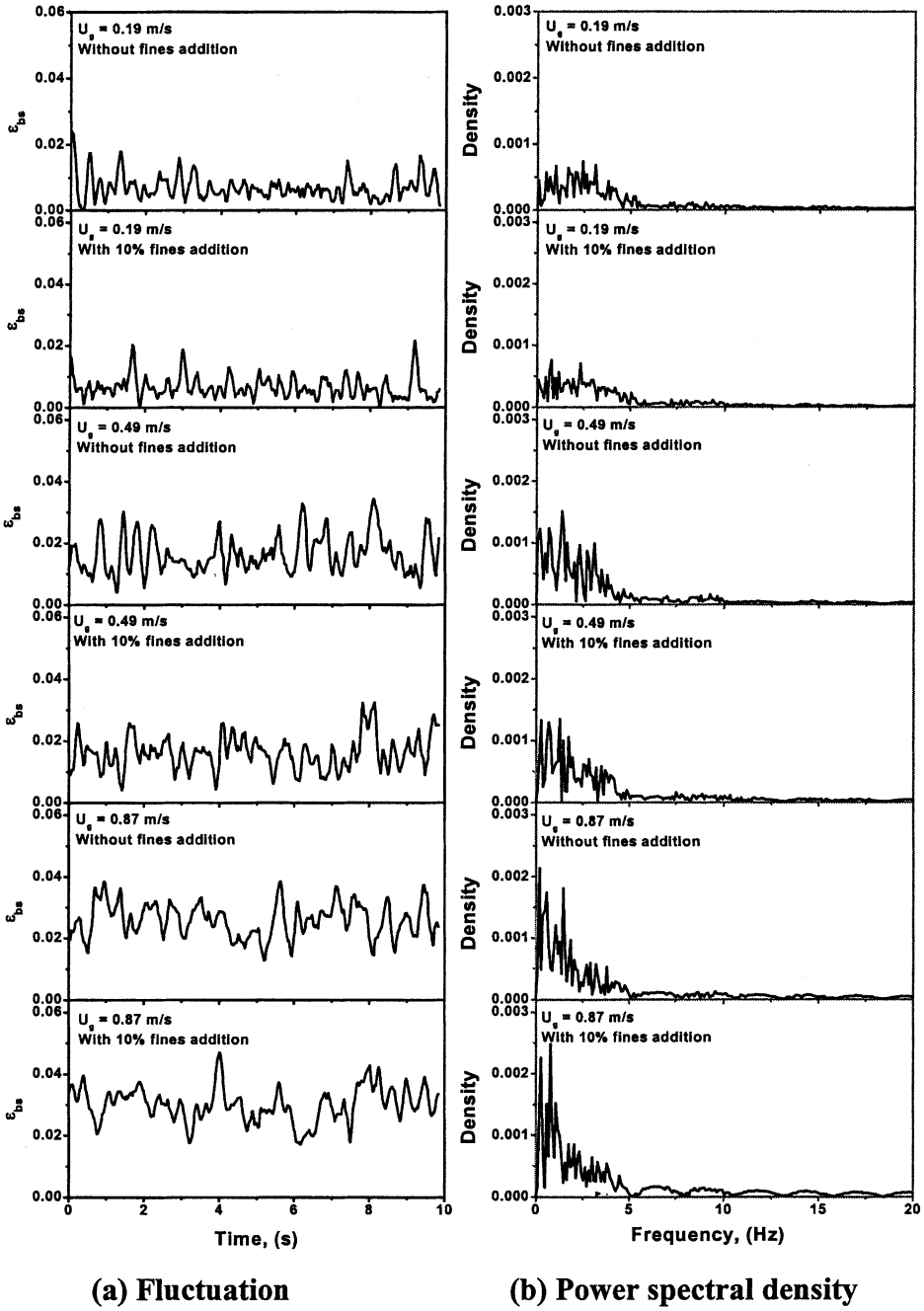

Figure 16. Fluctuations of cross-sectional averaged solids holdup in the bubble/void phase and their corresponding power spectral densities.

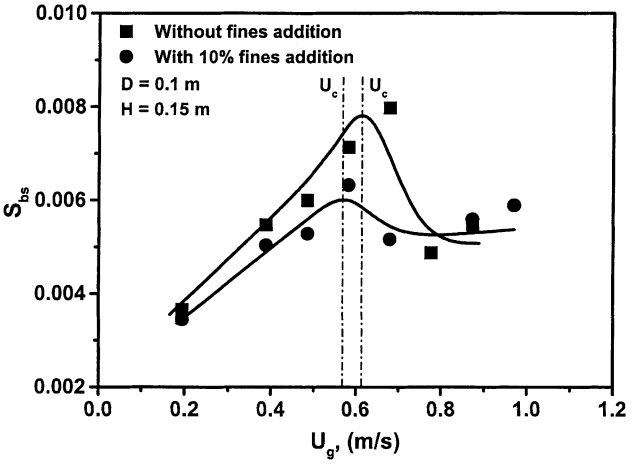

Figure 17. Standard deviation of the cross-sectional averaged solids holdup fluctuation in the bubble/void phase.

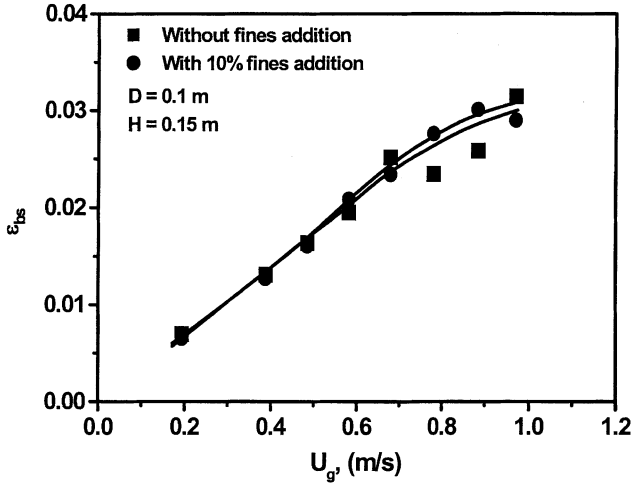

Figure 18. Variation of time-averaged solids holdup in the bubble/void phase with gas velocity.

phase was set at the peak value in the high solids concentration section of the probability density distribution. The 10% fines addition causes a decrease in the solids holdup in the emulsion phase in both the bubbling regime and the turbulent regime; this is also shown in Figure 21b. With the fines addition, fine particles tend to stay in the bubble/void phase. Furthermore, the entire bed, especially the emulsion phase, expands due to the breakup of larger bubbles or voids into smaller ones. In addition, the fine particles can be entrained easily and the elutriation of coarse particles is enhanced by the motion of fine particles (Geldart and Pope, 1983; Choi et al., 2001; Helland et al., 2001). These three factors contribute to the decrease in the solids holdup in the emulsion phase with fines addition. It is evident that the uniformity of fluidization is largely improved by the addition of fine particles based on the dynamic behavior and the time-averaged results shown for the bubble/void phase and the emulsion phase. Morse and Ballou (1951) presented similar results using the uniformity index defined in their study.

Effect of temperature on the phase structure measured by the optical fiber probe

The study on the effect of temperature on the dynamic behavior of gas-solid fluidization is carried out in a 0.2-m stainless steel fluidized bed using the optical fiber probe based on the combined threshold method described earlier. Comprehensive reviews on the effect of temperature on gas-solid fluidization have been reported in the literature (Yates, 1996; Smolders and Baeyens, 2000). Figures 22a and 22b show the effect of temperature on the time-averaged cross-sectional bubble/void phase fraction and solids holdup in the emulsion phase under the ambient pressure, respectively. It is seen that the variation of temperature has little effect on the bubble/void phase fraction both in the bubbling regime and in the turbulent regime. The solids holdup in the emulsion phase, however, decreases as the temperature increases from the ambient temperature to 150°C, and then levels off with the temperature. The cross-sectional solids holdup in the bed has a similar tendency. It is known that the bubble size decreases with temperature, which is reflected in the reduced magnitude of pressure fluctuations at high temperatures (Tone et al., 1974; Kai and Furusaki, 1985). Therefore, at higher temperatures, more homogeneous flow behavior is obtained due to the bubble size reduction and the emulsion phase expansion yielding a higher bed voidage. Kai and Furusaki (1985) also reported that the quality of fluidization improves as the temperature increases, resulting from the reduction in the bubble size. The changes in density and viscosity result in a steady decrease in the Galileo number with increasing temperature, which may partially elucidate the expansion of the emulsion phase at higher temperatures.

To explain and elucidate the results of the temperature effect on the flow behavior, a brief review of the literature is given here. Raso et al. (1992) studied the effect of temperature on the properties of the particulate phase at incipient fluidization. They found that, for Geldart group A particles, the variation of bed voidage at the incipient fluidization point with the temperature was determined only by the properties of the solid phase. Formisani et al. (1998) attributed the increase in bed voidage at minimum fluidization to the variation of the particulate mass properties with temperature. Rumpf (1977) studied the mechanisms of adhesion between particles. The adhesive force between particles was enhanced with increasing temperature. It is known that a high temperature just short of particle sintering results in viscoelastic deformation of the particles. Thus, viscous flattening of solid particles enlarged the interparticle contact area, strengthening the adhesive force between particles. Yamazaki et al. (1995) studied the effect of chemisorbed water on bed voidage of a high temperature fluidized bed and found that the humidity of the fluidizing gas played a significant role in determining the interparticle force. Because the Hamaker constant in water is smaller than in air, the adhesive force between particles was strengthened as dehydration proceeded with increasing temperature, resulting in an increase in the bed voidage at minimum fluidization. The behavior of the emulsion phase in the bubbling and the turbulent regimes is

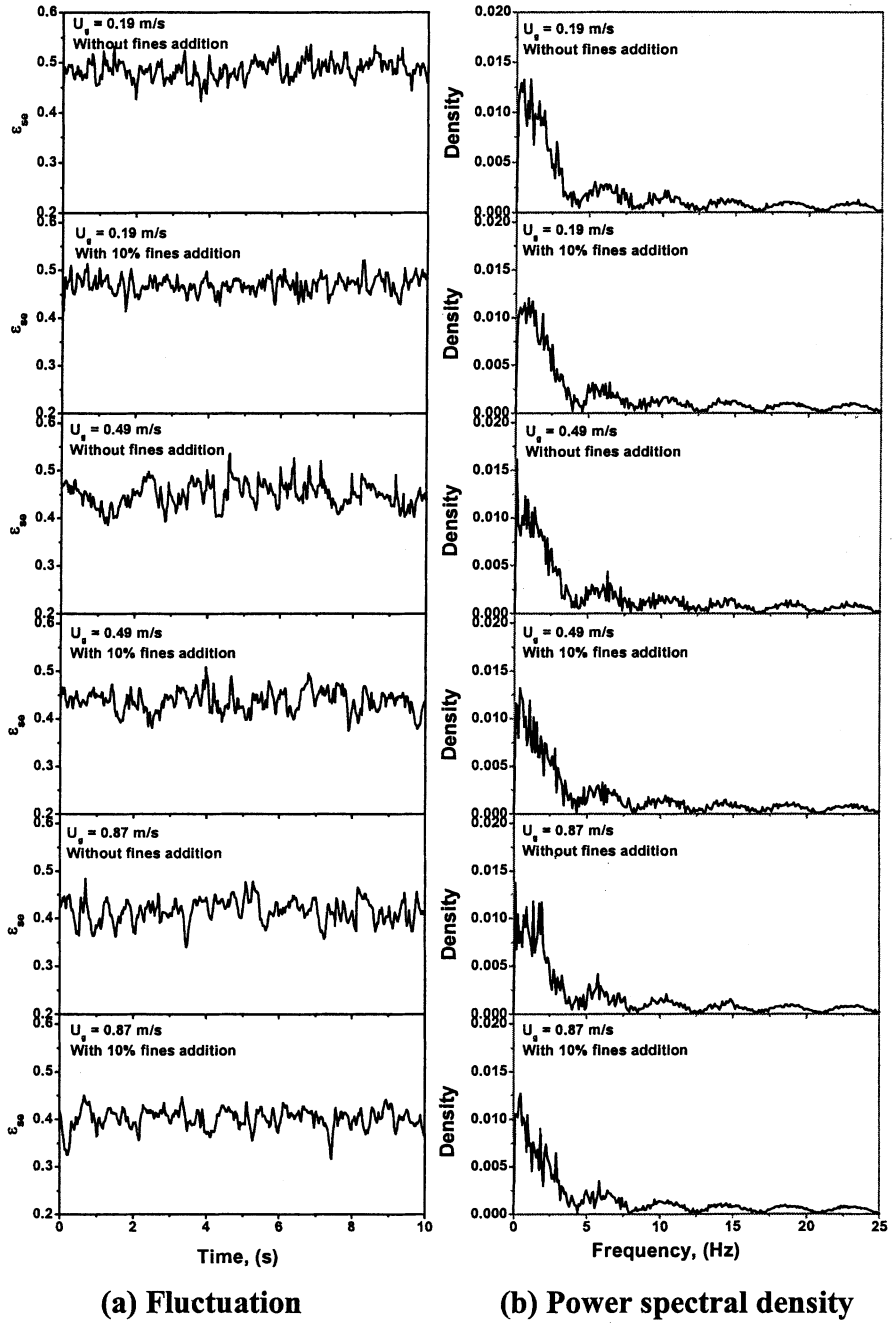

Figure 19. Fluctuations of cross-sectional averaged solids holdup in the emulsion phase and their corresponding power spectral densities.

similar to that of the particulate phase at incipient fluidization. The decrease of the solids holdup or the increase of the voidage in the emulsion phase needs to consider both the gas phase properties such as density, viscosity, and humidity, and the solid phase properties such as particle size, density, surface roughness, and content of impurities. Using the optical fiber probe, Farag et al. (1997) found that the temperature in the range of 22–135°C has a significant effect on the flow patterns of a pilot-scale turbulent fluidized bed. However, they found that the bubble fraction, bubble flow rate, bubble velocity, and bubble contact length all decrease significantly with an increase in temperature. Based on the literature and present work, it is clear that a more homogeneous flow at higher temperatures is closely linked to the behavior of an expanded emulsion phase with a higher bed voidage due to more gas transferring from the bubble phase to the emulsion phase.

Concluding Remarks

The neural network multicriteria optimization image reconstruction technique (NNMOIRT) developed by the au-

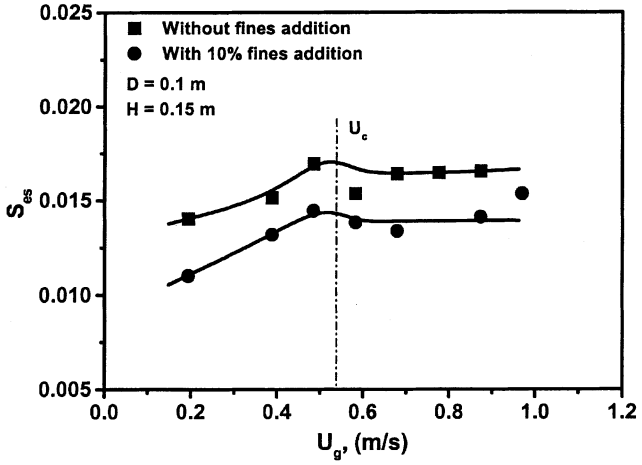

Figure 20. Standard deviation of the cross-sectional averaged solids holdup fluctuation in the emulsion phase.

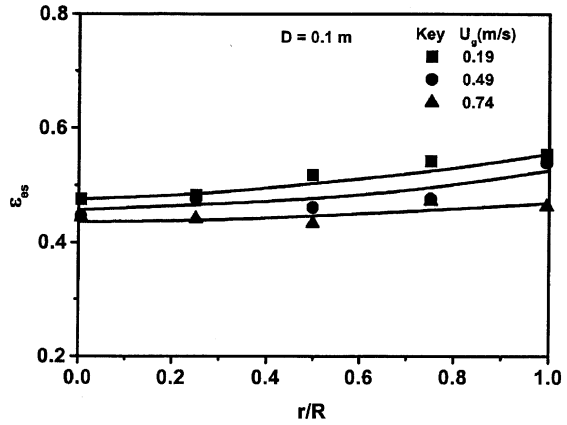

(a) Time-averaged radial variation of solids holdup in the emulsion phase

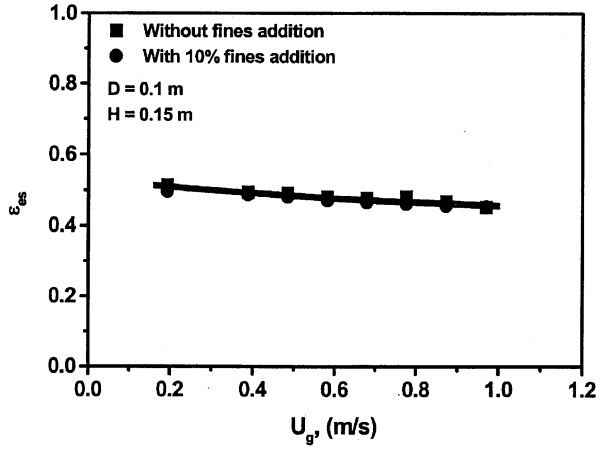

(b) Variation of time averaged cross-sectional solids holdup in the emulsion phase with gas velocity

Figure 21. Dynamic behavior of solids holdup in the emulsion phase.

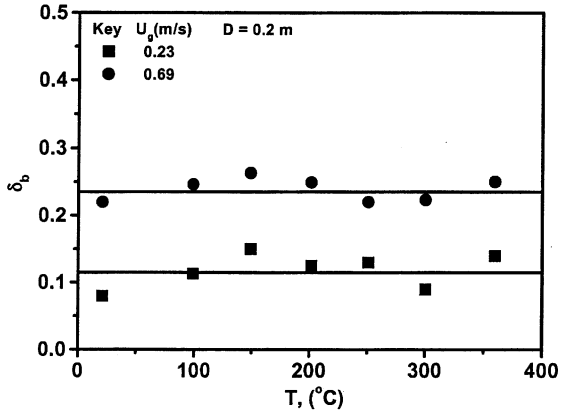

(a) Bubble/void phase fraction

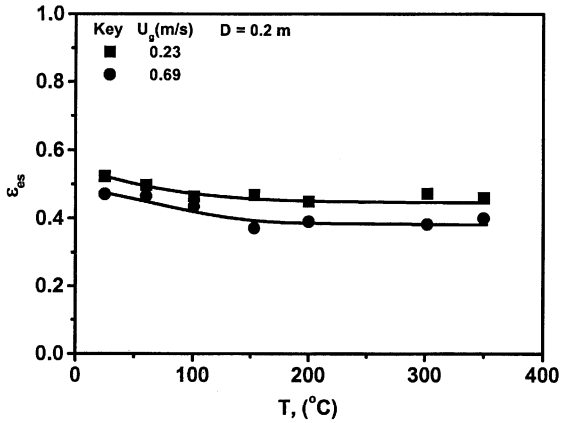

(b) Solids holdup in the emulsion phase

Figure 22. Effect of temperature on the bubble/void phase fraction and the solids holdup in the emulsion phase.

thors for the electrical capacitance tomography (ECT) applications provides a robust, real-time imaging of the cross-sectional dynamic behavior of a gas-solid fluidization system. The commonly employed optical fiber probe may yield significant error in defining the bubble/void phase and the emulsion phase and their holdups depending on the threshold level selected for the solids holdup distribution measured.

The ECT studies reveal a radial symmetry of the time-averaged solids holdup distribution for the turbulent regime. The standard deviation of the cross-sectional bubble/void phase fraction fluctuation and of the solids holdup fluctuation in the emulsion phase peaks at U_c, which further demonstrates the physical significance of the regime transition defined by U_c. The addition of 10% fine particles reduces the solids holdup in the emulsion phase due to the breakup of large bubbles to small bubbles or voids. At higher temperatures especially in the range of 25–150°C, the solids holdup in the emulsion phase measured by the optical fiber probe is reduced, which indicates an expanded emulsion phase with a higher bed voidage.

Acknowledgment

This article was presented as Paper No. 196d at the 2001 AIChE Meeting.

Notation

A_r = ring area at radial position r, m^2
d_b = bubble size, m
d_t = diameter of the bed, m
h = vertical distance from gas distributor, m
L_0 = length of the ECT electrode, m
L_b = length of a bubble, m
N = cross-sectional time-averaged output signal, V
N_r = time-averaged output signal at radial position r, V
R_b = radius of a bubble, m
R_c = radius of cloud surrounding a bubble, m
S_b = standard deviation of bubble/void phase fraction fluctuation
S_{bs} = standard deviation of solids holdup fluctuation in the bubble/void phase
S_{es} = standard deviation of solids holdup fluctuation in the emulsion phase
S_p = standard deviation of absolute pressure fluctuation
S_s = standard deviation of solids holdup fluctuation
U_{br} = rise velocity of single bubbles, m/s
U_c = transition velocity from the bubbling to turbulent regimes, m/s
U_f = upward velocity of gas at minimum fluidization, m/s
U_g = superficial gas velocity, m/s
U_{mf} = minimum fluidization velocity, m/s

Greek letters

δ_b = bubble/void phase fraction
δ_e = emulsion phase fraction
σ_c = standard deviation of solids fraction of cluster
ϵ_{bs} = solids holdup in the bubble/void phase
ϵ_{es} = solids holdup in the emulsion phase
$\underline{\epsilon_s}$ = solids holdup
ϵ_{sc} = average solids fraction of cluster
ϵ_{sm} = threshold value of solids holdup to distinguish the two phases
$\epsilon_{s,p}$ = solids concentration in a packed bed
ρ_b = bulk density, kg/m^3
ρ_g = gas density, kg/m^3
ρ_s = particle density, kg/m^3

Literature Cited

Abed, R., "The Characterization of Turbulent Fluid-Bed Hydrodynamics," *Fluidization IV*, D. Kunni and R. Toei, eds., Engineering Foundation, New York, 137 (1984).

Azzi, M., P. Turlier, J. F. Large, and J. R. Bernard, "Use of a Momentum Probe and Gammadensitometry to Study Local Properties of Fast Fluidized Beds," *Circulating Fluidized Bed Technology III*, P. Basu, M. Horio and M. Hasatani, eds., Pergamon, Oxford, 189 (1991).

Baeyens, J., and D. Geldart, "An Investigation into Slugging Fluidized Beds," *Chem. Eng. Sci.*, **29**, 255 (1974).

Bai, D., A. S. Issangya, and J. R. Grace, "Characteristics of Gas-Fluidized Beds in Different Flow Regimes," *Ind. Eng. Chem. Res.*, **38**, 803 (1999).

Bai, D., E. Shibuya, Y. Masuda, N. Nakagawa, and K. Kato, "Flow Structure in a Fast Fluidized Bed," *Chem. Eng. Sci.*, **51**(6), 957 (1996).

Bayle, J., P. Mege, and T. Gauthier, "Dispersion of Bubble Flow Properties in a Turbulent FCC Fluidized Bed," *Fluidization X*, M. Kwauk, J. Li and W.-C. Yang, eds., Engineering Foundation, New York, 125 (2001).

Beck, M. S., and R. A. Williams, "Process Tomography: a European Innovation and its Application," *Meas. Sci. Technol.*, **7**, 215 (1996).

Bi, H. T., and P. C. Su, "Local Phase Holdups in Gas-Solids Fluidization and Transport," *AIChE J.*, **47**(9), 2025 (2001).

Bi, H. T., N. Ellis, I. A. Abba, and J. R. Grace, "A State-of-the-Art Review of Gas-Solid Turbulent Fluidization," *Chem. Eng. Sci.*, **55**, 4789 (2000).

Brereton, C. M. H., and J. R. Grace, "Microstructure Aspects of the Behavior of Circulating Fluidized Beds," *Chem. Eng. Sci.*, **48**(14), 2565 (1993).

Cai, P., M. Schiavetti, G. DeMichele, G. C. Grazzini, and M. Miccio, "Quantitative Estimation of Bubble Size in PFBC," *Powder Technol.*, **80**, 99 (1994).

Cai, P., S. P. Chen, Y. Jin, Z. Q. Yu, and Z. W. Wang, "Effect of Operating Temperature and Pressure on the Transition from Bubbling to Turbulent Fluidization," *AIChE Symp. Ser.*, **270**, 37 (1989).

Chehbouni, A., J. Chaouki, C. Guy, and D. Klvana, "Characterization of the Flow Transition between Bubbling and Turbulent Fluidization," *Ind. Eng. Chem. Res.*, **33**, 1889 (1994).

Choi, J. H., J. M. Suh, I. Y. Chang, D. W. Shun, C. K. Yi, J. E. Son, and S. D. Kim, "The Effect of Fine Particles in Elutriation of Coarse Particles in a Gas Fluidized Bed," *Powder Technol.*, **121**, 190 (2001).

Cui, H., N. Mostoufi, and J. Chaouki, "Characterization of Dynamic Gas-Solid Distribution in Fluidized Beds," *Chem. Eng. Sci.*, **79**, 133 (2000).

Cui, H., N. Mostoufi, and J. Chaouki, "Gas and Solids between Dynamic Bubble and Emulsion in Gas-Fluidized Beds," *Powder Technol.*, **120**, 12 (2001).

Darton, R. C., R. D. LaNauze, J. F. Davidson, and D. Harrison, "Bubble Growth Due to Coalescence in Fluidized Beds," *Trans I ChemE*, **55**, 274 (1977).

Davidson, J. F., "Symposium on Fluidization-Discussion," *Trans. Instn. Chem. Engrs.*, **39**, 230 (1961).

Du, B., L.-S. Fan, F. Wei, and W. Warsito, "Gas and Solids Mixing in a Turbulent Fluidized Bed. "*AIChE J.*, **48**(9), 1896 (2002).

Dyakowski, T., L. Jeanmeure, and A. Jaworski, "Applications of Electrical Tomography for Gas-Solids and Liquid-Solids Flows–A Review," *Powder Technol.*, **112**, 174 (2000).

Dyakowski, T., R. B. Edwards, C. G. Xie, and R. A. Williams, "Application of Capacitance Tomography to Gas-Solid Flows," *Chem. Eng. Sci.*, **52**, 2099 (1997).

Farag, H. I., P. E. Ege, A. Grislingas, and H. I. DE Lasa, "Flow Patterns in a Pilot Plant-Scale Turbulent Fluidized Bed Reactor: Concurrent Application of Tracers and Fiber Optical Sensors," *Can. J. Chem. Eng.*, **75**, 851 (1997).

Formisani, B., R. Girimonte, and L. Mancuso, "Analysis of the Fluidization Process of Particle Beds at High Temperature," *Chem. Eng. Sci.*, **53**(5), 951 (1998).

Geldart, D., and D. J. Pope, "Interaction of Fine and Coarse Particles in the Freeboard of a Fluidized Bed," *Powder Technol.*, **34**, 95 (1983).

George, D. L., J. R. Torczynski, K. A. Shollenberger, T. J. O'Hern, and S. L. Ceccio, *Quantitative Tomographic Measurements of Opaque Multiphase Flows*, Sandia Report SAND2000-0441, Sandia National Laboratories, Albuquerque, NM (2000).

Hage, B., J. Werther, K. Narukawa, and S. Mori, "Capacitance Probe Measurement Technique of Local Particle Volume Concentration in Circulating Fluidized Bed Combustors," *J. Chem. Eng. Japan*, **29** (4), 594 (1996).

Helland, E., R. Occelli, and L. Tadrist, "Influence of the Presence of Fines on the Fluidisation of Large Particles," *Multi-Phase Flow Transp. Phenom., Int. Symp.*, 364 (2001).

Kai, T., and S. Furusaki, "Behavior of Fluidized Beds of Small Particles at Elevated Temperatures," *J. Chem. Eng. Japan*, **18**(2), 113 (1985).

Kumar, S. B., D. Mosleman, and M. P. Dudukovic, "Gas-Holdup Measurements in Bubble Columns Using Computed Tomography, *AIChE J.*, **43**, 1414 (1997).

Kunni, D., and O. Levenspiel, *Fluidization Engineering*, 2nd ed., Butterworth-Heinemann, Boston (1991).

Lin, Q., F. Wei, and Y. Jin, "Transient Density Signal Analysis and Two-Phase Micro-Structure Flow in Gas-Solids Fluidization," *Chem. Eng. Sci.*, **56**, 2179 (2001).

Malcus, S., and T. S. Pugsley, "Investigation of the Axial Variation of the CFB Riser Hydrodynamics by Means of Electrical Capacitance Tomography (ECT)," *Fluidization X*, M. Kwauk, J. Li, and W.-C. Yang, eds., Engineering Foundation, New York, 763 (2001).

Morse, R. D., and C. O. Ballou, "The Uniformity of Fluidization—Its Measurement and Use," *Chem. Eng. Prog.*, **47**(4), 199 (1951).

Nakajima, M., M. Harada, M. Asai, R. Yamazaki, and G. Jimbo, "Bubble Fraction and Voidage in an Emulsion Phase in the Transition to a Turbulent Fluidized Bed," *Circulating Fluidized Bed III*, P. Basu, M. Horio and M. Hasatani, eds., *Pergamon*, Oxford, 79 (1991).

Raso, G., M. D'Amore, B. Formisani, and P. G. Lignola, "The Influence of Temperature on the Properties of the Particulate Phase at Incipient Fluidization," *Powder Technol.*, **72**, 71 (1992).

Rowe, P. N., "Experimental Properties of Bubbles," *Fluidization*, J. F. Davidson and D. Harrison, eds., Academic Press, New York, 121 (1971).
Rowe, P. N., "Prediction of Bubble Size in a Gas Fluidized Bed," *Chem. Eng. Sci.*, **31**, 285 (1976).
Rumpf, H., "Particle Adhesion," *Agglomeration 77*, *Proc. Int. Symp.*, 2nd ed., **1**, 97 (1977).
Seville, J. P. K., J. E. P. Morgan, and R. Clift, "Tomographic Determination of the Voidage Structure of Gas Fluidized Beds in the Jet Region," *Fluidization V*, K. Østergaard and A. Sørensen, eds., Engineering Foundation, New York, 87 (1986).
Smolders, K., and J. Baeyens, "Fluidization at Elevated Temperature and/or Pressure," *Powder Handl. Process.*, **12**, 47 (2000).
Smolders, K., D. Geldart, and J. Bacyens, "The Physical Models of Cyclone Diplegs in Fluidized Beds," *Chinese J. Chem. Eng.*, **9**, 337 (2001).
Sun, G. L., and J. R. Grace, "The Effect of Particle-Size Distribution on the Performance of a Catalytic Fluidized-Bed Reactor," *Chem. Eng. Sci.*, **45**, 2187 (1990).
Tone, S., H. Seko, H. Maruyama, and T. Otake, "Catalytic Cracking of Methylcyclohexane over Silica Alumina Catalyst in Gas Fluidized Bed," *J. Chem. Eng. Japan*, **7**, 44 (1974).
Warsito, W., and L.-S. Fan, "Measurement of Real-Time Flow Structures in Gas-Liquid and Gas-Liquid-Solid Flow Systems using Electrical Capacitance Tomography (ECT)," *Chem. Eng. Sci.*, **56**, 6455 (2001a).
Warsito, W., and L.-S. Fan, "Neural Network Based on Multi-Criteria Optimization Image Reconstruction Technique for Imaging Two- and Three-Phase Flow Systems Using Electrical Capacitance Tomography," *Meas. Sci. Technol.*, **12**, 2198 (2001b).
Warsito, W., M. Ohkawa, N. Kawata, and S. Uchida, "Cross-Sectional Distributions of Gas and Solid Holdups in Slurry Bubble Column Investigated by Ultrasonic Computed Tomography, *Chem. Eng. Sci.*, **54**, 4711 (1999).
Werther, J., Bubble Growth in Large Diameter Fluidized Beds," *Fluidization Technology: Proc. of the Int. Fluidization Conf.*, D. L. Keairns, ed., Asilomar, CA, **1**, 215 (1976).
Werther, J., "Measurement Techniques in Fluidized Beds," *Powder Technol.*, **102**, 15 (1999).
Werther, J., and J. Wein, "Expansion Behavior of Gas Fluidized Beds in the Turbulent Regime," *AIChE Symp. Ser.*, **301**, 31 (1994).
Wiesendorf, V., and J. Werther, "Capacitance Probes for Solids Volume Concentration and Velocity Measurements in Industrial Fluidized Bed Reactors," *Powder Technol.*, **110**, 143 (2000).
Yamazaki, R., N. S. Han, Z. F. Sun, and G. Jimbo, "Effect of Chemisorbed Water on Bed Voidage of High Temperature Fluidized Bed," *Powder Technol.*, **84**, 15 (1995).
Yang, W. Q., and S. Liu, "Role of Tomography in Gas/Solids Flow Measurement," *Flow Meas. Instrum.*, **11**, 237 (2000).
Yates, J. G., "Effects of Temperature and Pressure on Gas-Solid Fluidization," *Chem. Eng. Sci.*, **51**, 167 (1996).
Yates, J. G., and S. J. R. Simons, "Experimental Methods in Fluidization Research," *Int. J. Multiphase Flow*, **20**, Suppl., 297 (1994).
Yerushalmi, J., and N. T. Cankurt, "Further Studies of the Regimes of Fluidization," *Powder Technol.*, **24**, 187 (1979).
Zhang, W., F. Johnsson, and B. Leckner, "Characteristics of the Lateral Particle Distribution in Circulating Fluidized Bed Boilers," *Circulating Fluidized Bed Technology IV*, A. A. Avidan, ed., AIChE, New York, p. 266 (1994).
Zhang, X., Y. Qian, S. Guo, and Y. Zhang, "Application of the Optical Fiber Probe to the Measurement of the Bubble Characteristics in a Turbulent Fluidized Bed with FCC Particles," *Huanan Ligong Daxue Xuebao, Ziran Kexueban*, (in Chinese), **25**, 20 (1997).

Manuscript received Apr. 2, 2002, revision received Dec. 9, 2002, and final revision received Feb. 18, 2003.